Testing of self-similarity and helical symmetry in vortex generator flow simulations

Unai Fernández-Gámiz[1], Clara Marika Velte[2], Pierre-Elouan Réthoré[3], Niels N. Sørensen[3] and Eduard Egusquiza[4]

[1] Nuclear Engineering and Fluid Mechanics Department, University of the Basque Country, Nieves Cano 12, 01006 Vitoria-Gasteiz, Araba, Spain

[2] Section of Fluid Mechanics, Coastal and Maritime Engineering,Department of Mechanical Engineering, Technical University of Denmark, Nils Koppels Allé, 2800 Kgs. Lyngby, Denmark

[3] DTU Wind Energy Department, Technical University of Denmark, Risø Campus, Bldg 115, Frederiksborgvej 399, DK-4000 Roskilde, Denmark

[4] Technical University of Catalonia, Fluid Mechanics Department, Av. Diagonal 647, 08028 Barcelona, Spain.

ABSTRACT

Vortex generators (VGs) are used increasingly by the wind turbine industry as flow control devices to improve rotor blade performance. According to experimental observations, the vortices generated by VGs have previously been observed to be self-similar for both the axial (u_z) and azimuthal (u_θ) velocity components. Furthermore, the measured vortices have been observed to obey the criteria for helical symmetry. These are powerful results, as it reduces the highly complex 3-D flow to merely four parameters and therefore significantly facilitates the modeling of this type of flow, which in a larger perspective can assist in parametric studies to increase the total power output of wind turbines. In this study, corresponding computer simulations using Reynolds-averaged Navier–Stokes equations have been carried out and compared with the experimental observations. The main objective is to investigate how well the simulations can reproduce these aspects of the physics of the flow, i.e., investigate if the same analytical model can be applied and therefore significantly facilitate the modeling of this type of flow, which in a larger perspective can assist in parametric studies to increase the total power output of wind

turbines. This is especially interesting since these types of flows are notoriously difficult for the turbulence models to predict correctly. Using this model, parametric studies can be significantly reduced, and moreover, reliable simulations can substantially reduce the costs of the parametric studies themselves.

KEYWORDS

vortex generator; wake; CFD; computational fluid dynamics; aerodynamics; wind turbine

Correspondence

U. Fernández-Gámiz, Nuclear Engineering and Fluid Mechanics Department, University of the Basque Country, Nieves Cano 12, 01006 Vitoria-Gasteiz, Araba, Spain.

E-mail: unai.fernandez@ehu.es

1. INTRODUCTION

Research has been carried out on vortex generators (VGs) in applied aerodynamics on airplane wings for more than 60 years.[1–3] VGs are passive devices for flow control that enhance mixing of the boundary layer and can thus transfer high- momentum fluid closer to the wall and thereby suppress separation.[4] An extensive range of conventional VGs is in use for successful engineering applications of flow separation control, since controlled near-wall vortices can transport both heat and momentum, aiding in cooling and re-energizing the lowest part of the boundary layer. The fluid particles with great streamwise momentum are swept along helical trajectories toward the surface to mix with and, to some extent, to restore the retarded near-wall flow. Therefore, it is important to be able to control and optimize parameters such as the vortex strength and vortex core size to the existing flow setting.[5] On wind turbine blades, VGs are usually mounted in a spanwise array on the suction side of the blade and have the advantage that they can be added as a post-production fix to blades that do not perform as expected. An overview of different airfoils with several VG options is listed by van Rooij *et al.*[6] They are further frequently employed on, e.g., wind turbine blades to enable production of more slender

blades. That is, the width of a blade can be reduced, thereby also reducing the weight for the same load distribution and power production and thus facilitating upscaling of the turbines.

These devices are commonly triangular or rectangular vanes inclined at an angle of attack to the oncoming flow. They are normally dimensioned in relation to the local boundary layer thickness to obtain optimal interaction between the vortex and boundary layer and are frequently arranged in pairs, producing counter-rotating vortices, upstream of the flow separation

area.[7, 8] Basic research on VGs mounted on a flat plate has previously been the concern of several researchers (e.g., Lin[7]).

For an example of successful control of a laminar separation bubble with significant drag reduction, see the research at moderate Reynolds number carried out by Kerho *et al.*[9] Also, Lin[7] observed the drag-reducing and lift-increasing effects of micro VGs. Wendt[10] investigated an array of VGs in an experiment where the VGs were mounted in a fashion to generate counter-rotating vortices. Furthermore, the experimental and numerical studies carried out by Ashill *et al.*[11, 12] revealed a successful delaying of the shock-induced separation by the implementation of sub-boundary-layer VGs. Two series of investigations were presented at both zero and adverse streamwise pressure gradients, where vortex decay and device drag were reasonably well predicted by the Reynolds-averaged Navier–Stokes (RANS)-based computations.

The effect of VGs on a 1 MW wind turbine was investigated by Øye[13] and Miller,[14] who compared the measured power curves on a (however optimistically designed) wind turbine with and without VGs. Although quite rough methods for the optimization of the VG design were employed, these studies showed that in the case under investigation the VGs on average increased the output power for nearly all wind speeds. Adding VGs to wind turbine blades is often a simple measure to improve the performance of a rotor, although great care needs to be taken not to deteriorate the performance of the wind turbine or, even worse, to change the aeroelastic performance adversely so that the wind turbine becomes destabilized. This can significantly reduce the lifetime of the wind turbine, which further highlights the need for proper models of VGs.

Many models for the generated vortices have been presented over the years. Theoretical models include, for example, the one by Smith[15] and a model presented by Velte *et al.*[5]

that was developed and applied to show the helical symmetry of the vortices generated by a passive rectangular vane-type VG. As for more practically and numerically oriented mod- els incorporated into codes, most are variants of the practical Bender–Anderson–Yagle model by Bender *et al.*,[16] which introduces body forces using source terms in the Navier–Stokes equations to simulate the presence of a vane.

The fact that the vortices produced by VGs possess helical symmetry means, in effect, that the streamwise profiles (u_z), along the longitudinal vortex axis, and the rotational (u_0) flows are inter-related by a simple linear relation based on the helical shape of the vorticity lines.[5, 17] Further, previous experimental work by Velte[18] examines the downstream vortex evolution behind a cascade of VGs producing counter-rotating vortices in a boundary layer of negligible streamwise pres- sure gradient. The model parameters are all seen to vary linearly in the downstream direction. Based on the experimental observations of Velte,[18] the vortices generated by VGs have been observed to be self-similar (e.g., White[19] and Figure 1)
for both the axial (u_z) and azimuthal (u_0) velocity profiles. If the flow, i.e., the set of four helical parameters (u_0, l, I' and "), is known at one single position, the flow can therefore be extended to include the full downstream evolution of the devel- oped part of the vortex using self-similarity scaling arguments. This knowledge is important for fundamental understanding
as well as for the aspect of applications, for which parametric experiments can be substantially reduced in terms of required time and cost. This would, in turn, simplify the process of improving existing wind turbine designs using retrofits or the upscaling of wind turbines, as described earlier. Note that, in practice, VGs are often optimized using computational fluid dynamics (CFD) methods because of the relatively low cost and fast acquisition of the results. However, the performance

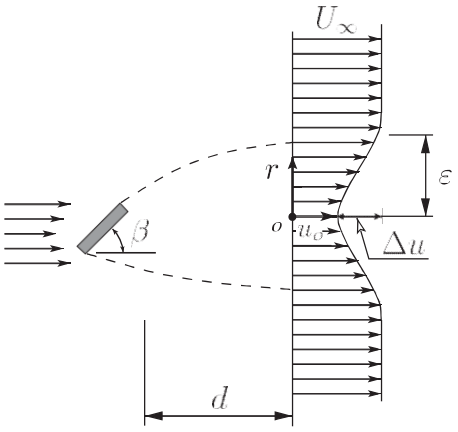

Figure 1. Wake velocity profile of a single VG at a distance d from the trailing [1] edge of the vane with free stream velocity U and convection velocity u_0. Δu and ε represent the characteristic velocity scale and the characteristic shear-layer width, respectively.

of CFD codes to predict this complex wall-bounded flow correctly still remains to be properly validated, and the present study therefore suggests a quantitative method comparing experimental and computational results describing the complete set of aspects describing the VG-induced wake. Hence, before attempting the extremely complex 3-D and rotating flow on a wind turbine blade, the present study based on a more simple setup can be used as a preliminary orientation for suc- cessful implementation of VGs on wind turbine rotor blades. To the knowledge of the authors, this kind of comparison has previously only been performed in a qualitative fashion or only quantitatively to some extent.

In the present study, CFD simulations have therefore been carried out using the DTU/RISØ in-house EllipSys3D CFD code[20, 21] and compared with wind tunnel experiments, where a test case was performed over a single vane mounted on the test section wall in a low-speed wind tunnel.[18] The main objective of this work is to investigate how well the simulations can reproduce the physics of the flow and if the same analytical model can be applied to the computer-simulated results. The results show that CFD is able to capture the same overall flow trends as the measured ones. Using this model, parametric studies can be significantly reduced, and furthermore, reliable simulations can

substantially reduce the costs and time requirements of the parametric studies themselves.

2. COMPUTATIONAL CONFIGURATION

In this study, steady-state simulations were carried out and compared with experimental observations. These computations were performed using the EllipSys3D code.[20, 21] This in-house CFD code is a structured finite-volume flow solver using, in this work, RANS equations. The pressure/velocity coupling is ensured using the Semi-implicit Method for Pressure Linked Equations algorithm. The convective terms are discretized by utilizing the third-order Quadratic Upstream Interpolation for Convective Kinematics.[22] For these computations, the k ! shear stress transport turbulence model by Menter[23] was used. A successful validation of steady RANS simulations against measurements is the one carried out by Allan,[24] where the flow field about a single VG on a flat plate with two different vane angles of attack was computed using a flow solver code developed at the National Aeronautics and Space Administration. The results of these simulations were compared with experimental data and showed that the CFD and experiments agreed well except for short distances downstream of the vane.

Figure 2 illustrates the computational setup with the current setting consisting of a single VG on a flat plate. The actuator is a rectangular vane with a length two times the VG height. The computational domain with dimensions normalized with the VG height is also given in Figure 2, as also described more in detail by Menter.[25] The thickness of the vane is constant,

and the VG was positioned directly on the wall at a position where the boundary layer thickness is equal to the VG height. The data were extracted in five spanwise planes, normal to the test section floor and located 5, 7.5, 10, 12.5 and 15 VG heights downstream of the VG trailing edge.

The computational setup was designed to mimic that of the experiments.[18] The VG angle of attack to the oncoming

flow is 20¹, and the Reynolds number based on VG height h 0.25 m is Re 1700, using an inflow velocity of U 1 ms^{-1} and a density of 1 kg m^{-3}. At the bottom wall and on the VG surface, no-slip conditions were specified, while the upstream and lid part of the domain were specified as inflow conditions with prescribed velocity according

to the

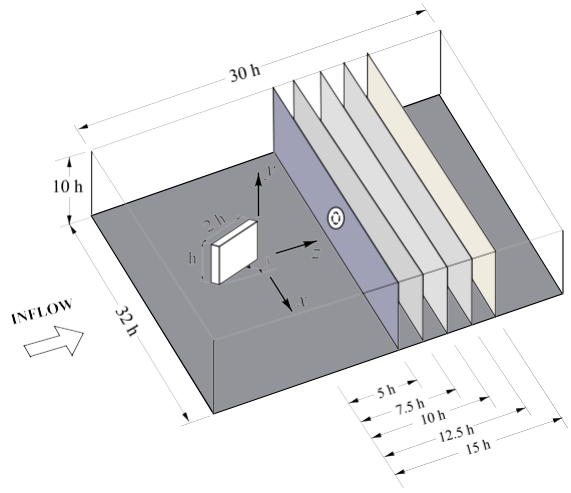

Figure 2. Computational domain (not to scale).

undisturbed velocity. The two side faces of the domain were specified as slip/symmetry conditions, while the downstream plan was set as an outlet assuming a fully developed flow. At the inlet, the turbulence is set to give very low eddy viscosity, and the turbulence seen by the VG is generated by the developing boundary layer along the wall surface.

In the experiments, the turbulence intensity at the inlet from laser Doppler anemometry (LDA) measurements was found to be 13% where the turbulence was generated by a grid at the inlet. The boundary layer thickness at the position of the VGs was estimated from LDA measurements to be approximately $_1VG$ D 25 mm. The actuators were rectangular vanes of the same height as the local boundary layer thickness, h $_1VG$, with a length of 2h. The computations have been carried out based on the experimental inflow profile illustrated in Figure 3. This figure represents the measured (stereoscopic particle image velocimetry) turbulent boundary layer profile without VG at the position where the VG was later mounted. A more complete characterization of the inlet conditions can be found in the PhD thesis of Velte.[26]

The computational setup of the CFD simulations consists of a block-structured mesh of 18 million cells with the first cell height (z=h) of 1.5 10^{-6} normalized by the VG height. In the immediate vicinity of the vane, the mesh has 5 10^6 cells, while the mesh downstream the VG for capturing the wake has approximately 2.5 10^6 cells. In order to

resolve the boundary layer, cell clustering has been used close to the wall, and the dimensionless distance from the wall is less than 1 ($y^C < 1$), as is required by the shear stress transport turbulence model.

Verification of sufficient mesh resolution was performed by a mesh dependence study. Results obtained for the finer mesh level 1 (66 blocks of 64^3 cells) are compared with results obtained for a standard level 2 (66 blocks of 32^3 cells) and a coarser mesh level 3 (66 blocks of 16^3 cells). As a grid stretching method, the hyperbolic tangent stretching function of Vinokur[27] was used. Figure 4 illustrates the axial and azimuthal velocity profiles for three grid levels. These profiles were extracted in a plane normal to the flow direction at five VG heights downstream of the vane and along a line parallel to the wall passing through the center of the primary vortex. Mesh dependence of less than 6% has been detected for both axial and azimuthal velocities. The simulations were converged until a satisfactory residual convergence was achieved on the velocities, pressure and turbulence quantities.

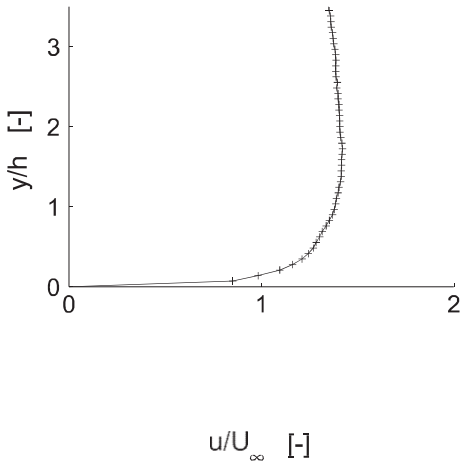

Figure 3. Inflow profile measured using stereoscopic particle image velocimetry at the position of the VG without the VG present.

[-]

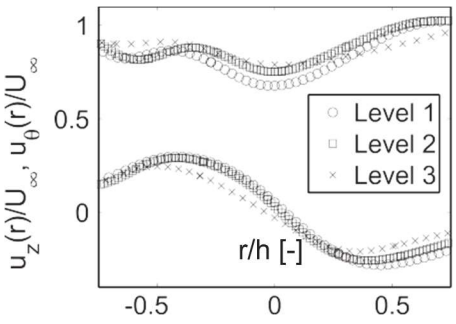

Figure 4. Axial and azimuthal velocity profiles for three different mesh sizes of the computations.

3. RESULTS

The analysis of helical symmetry was performed on computational results extracted in the cross planes positioned at $z=h$ 5, 7.5, 10, 12.5 and 15 VG heights downstream of the trailing edge of the VG. The reason for the analysis not to be performed at positions closer to the VG is that the wake in this range is still forming and therefore has not yet developed the helical symmetry (see also Velte[18, 26]). An angle of attack of ˘ 20¹ of the VG to the oncoming flow was chosen for the computations and subsequently compared with the wind tunnel experiments and the analytical model by Velte.[18] The vane angle is close to the optimum found by Godard *et al.*[28] in a parametric study optimizing separation control. The extraction of velocities from the computations was conducted in a similar way to the experimental procedure described by Velte *et al.*,[5] in planes normal to the section wall downstream of the VG and applying polar coordinates $(z, r, 0)$ to the vortex with the origin at the vortex center.

3.1. Testing of helical symmetry

The first necessary step is to check whether the simulation results fulfill helical symmetry. In order to perform this test, the three velocity components were extracted along lines passing through the center of the primary vortex at four angles of ¸ .0¹, 45¹, 90¹ and 135¹) to cover the full rotational variations of the vortex (Figure 5). The cylindrical coordinate system used to describe these variations across the vortex core is presented in Figure 5, with the center always located at the vortex core center. The origin of the z-axis is located at the upper edge of the VG trailing edge.

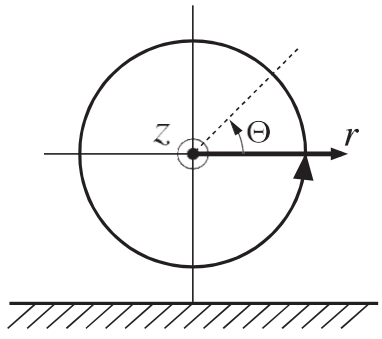

Figure 5. Polar coordinate system centered at the vortex core center.

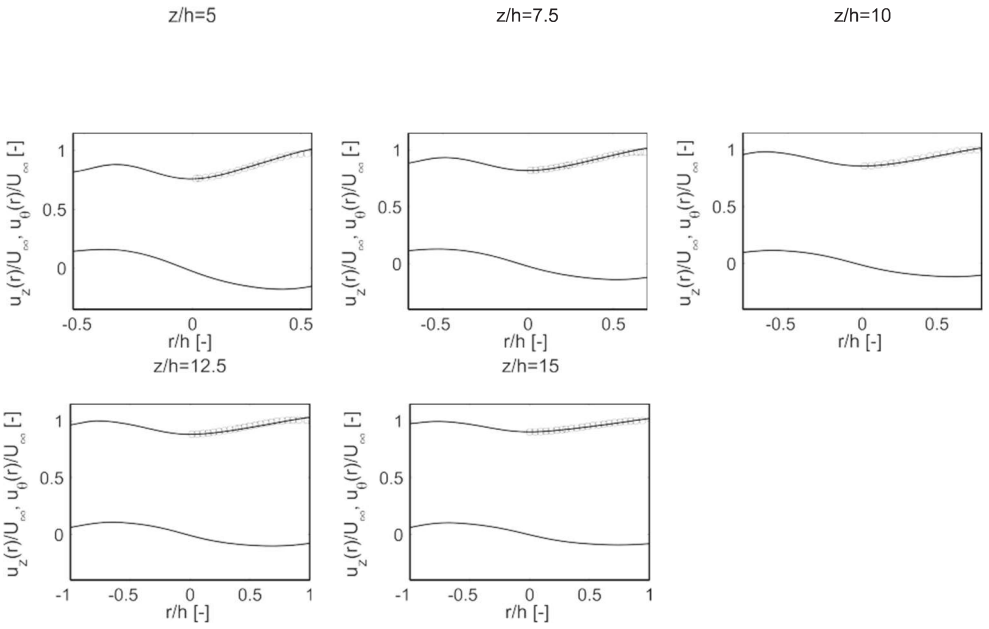

Figure 6. CFD velocity profiles of embedded vortices generated by a VG for a device angle ˇ D 20¹ and ¸ D 0¹. The negative *r=h* values represent the *r=h* axis for ¸ D 180¹. Upper values are the axial velocity profile *uz* and lower the azimuthal one u_e normalized by *U* . For positive *r=h*, CFD values of *uz* are compared with the right-hand side of equation (1) calculated using the computational values u_0 and u_e (°).

The solid curves in Figure 6 illustrate the axial and azimuthal velocity profiles (upper curves are the axial velocity profile u_z and lower the azimuthal one u_0) for each plane position where the data are extracted along a horizontal line through the vortex center. These curves are compared with what is obtained from the right-hand side of equation (1), finding l by least squares fitting of the residual.[18] The two data sets overlap well for all plane positions, confirming that the computational results fulfill the criterion for helical symmetry just like the experimental ones do. Note that the analysis has been carried out only on the right side, owing to a perturbing secondary vortex appearing on the left side yielding an asymmetric velocity profile.[5]

$$u_z \mathrm{D} u_0 - {}^{r}\!/_{l} u_0 \tag{1}$$

Figure 7 displays the streamwise evolution of the helical parameters that directly result from this analysis: vortex convection velocity (u_0), circulation (r), helical pitch (l) and vortex core radius (") for the wind tunnel experiments and computational simulations. The error bars illustrate the error of the linear fit to the data. The local flow char- acteristic u_0 was found directly from the lowest value of the axial velocity wake profile in the vortex core, and the helical pitch l was obtained from least squares fitting of equation (1). The circulation has been calculated from inte- gration as the flux of vorticity across a surface enclosed by a curve described by the vortex radius. The vortex core radius " has been obtained as the radius of the maximum value of the azimuthal velocity for each plane position. For a better comparison between the experimental and computational results, both vortex radius and helical pitch have

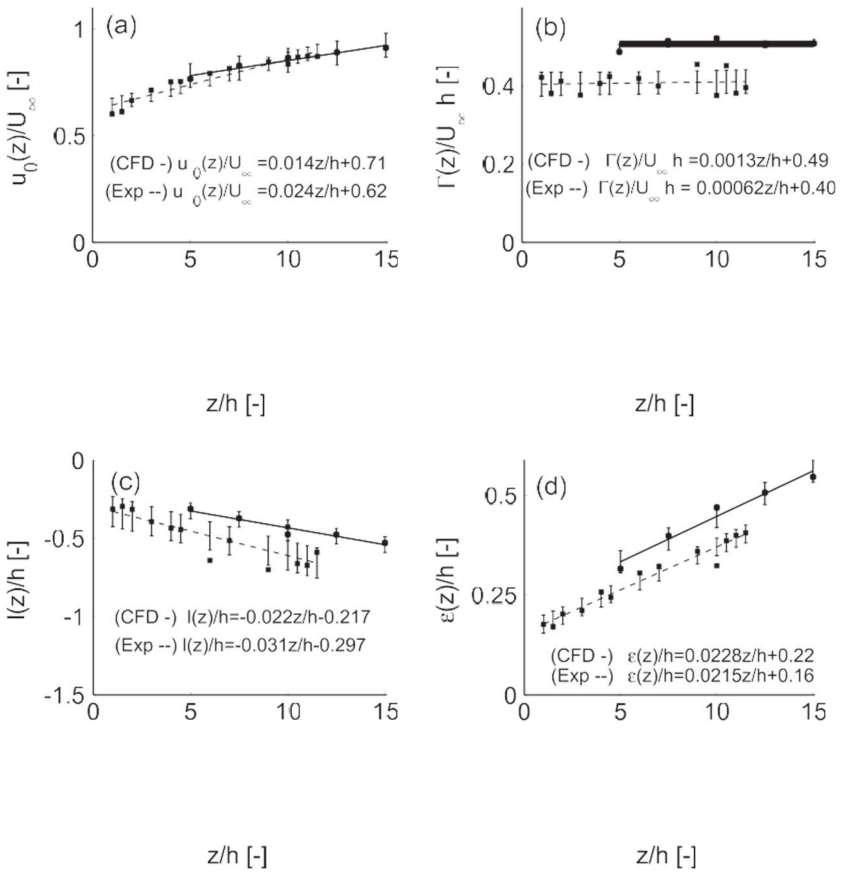

Figure 7. Comparison between CFD and experimental results of the downstream evolution of the characteristic vortex parameters.

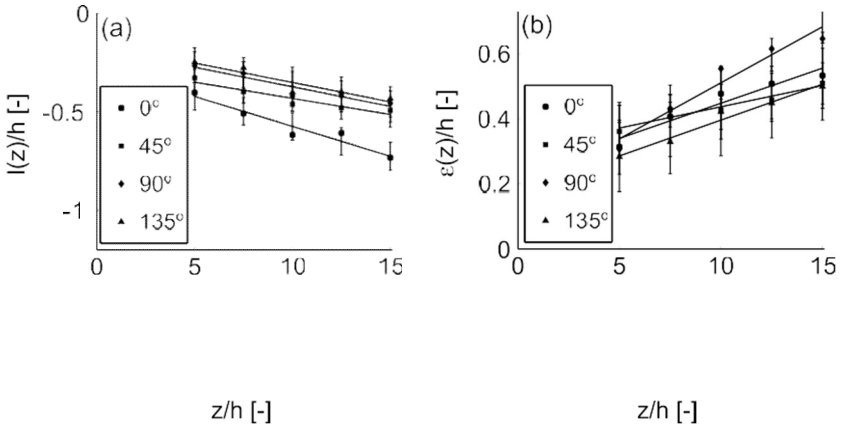

Figure 8. CFD results of the downstream evolution of the helical pitch (a) and the vortex radius (b) at different angles of ¸: 0¹, 45¹, 90¹ and 135¹.

been normalized by the VG height *h* and averaged across the azimuthal coordinate ¸. To illustrate the helical param- eter dependence on ¸, Figure 8 was represented. This figure provides the CFD results of the evolution downstream of the VG for the helical pitch *l* and the vortex core radius " at different angles of ¸. The convection velocity has been normalized by the free stream velocity U_1 and the circulation by the product $U_1 h$. Since the axial and azimuthal veloc- ities are observed to be self-similar, it is expected that u_0 and *l* also vary linearly along the downstream path, which is indeed observed for both the experiments and the simulations in Figure 7. As expected, the only factor that does not vary along the plane positions is the circulation, which should naturally be close to constant in a system of low viscous dissipation.

In fact, all helical parameters are seen to vary linearly with the downstream distance, for both experiments and simula- tions. Further, the general trends agree in the downstream evolution of all parameters, although the absolute values differ between the quantities. As pointed out earlier, the vortex strength is larger in the simulations, and the vortex core size is also somewhat larger and varies with a steeper gradient in the downstream direction. The normalized convection velocity $u_0=U_1$ (minimum axial velocity at the center of the vortex core divided by the free stream velocity) in the downstream

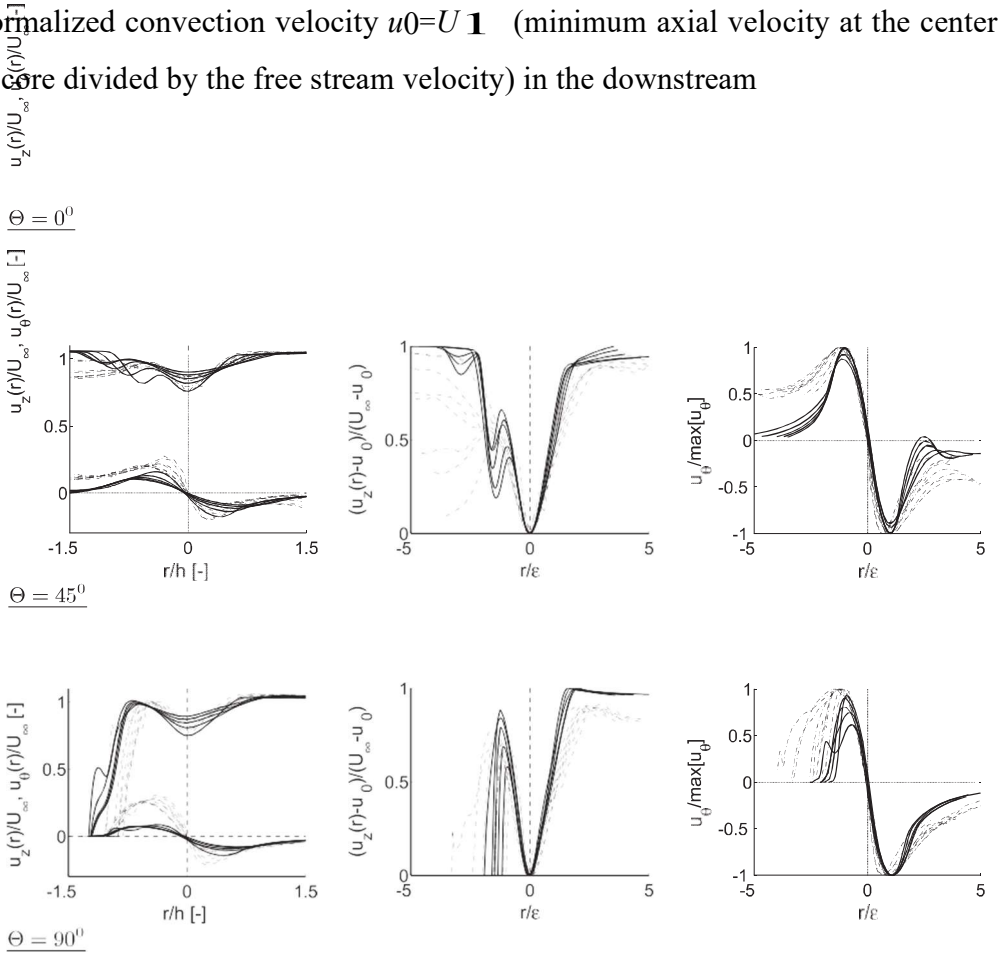

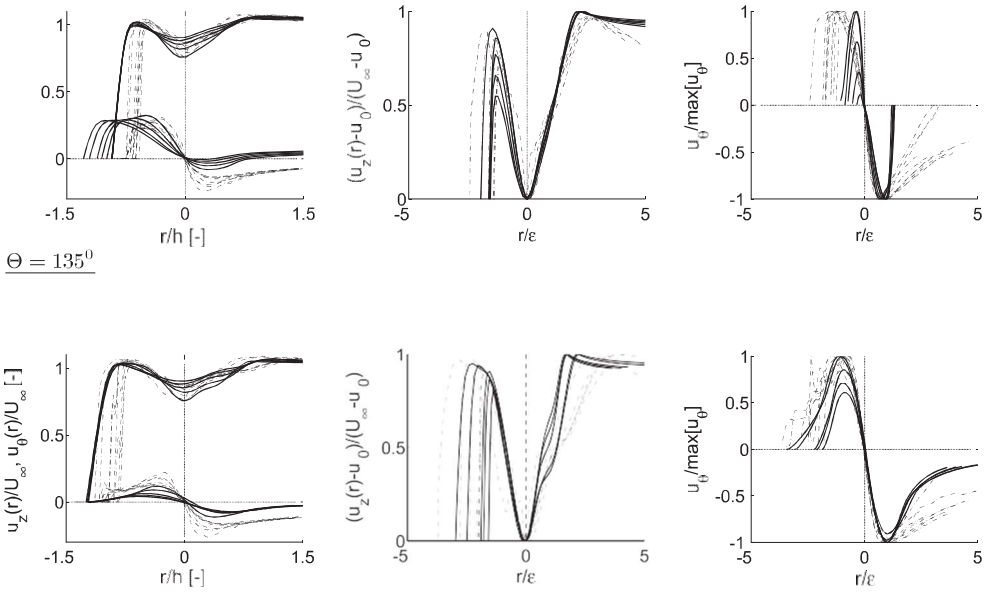

Figure 9. CFD (solid lines) and experimental (dash-dotted lines) velocity profiles for various angles , at different plane positions downstream of the VG. The left side shows the axial (uz) and azimuthal (u_θ) profiles, and the middle and right sides show the axial and azimuthal profiles, respectively, scaled by self-similarity variables.

direction was also observed to be smaller in the measurements for the positions closer to the VG, while in the positions far away from the trailing edge of the VG, it is larger in the measurements in comparison with the CFD results (Figure 7). This means that the axial velocity induction caused by the helical vorticity lines is stronger in the measurements far away from the VG. The relation between the convection velocity and the helical pitch is not as straightforward though, since the strength of the vorticity lines may vary.

3.2. Testing of wake self-similarity

Figure 9 displays the axial (u_z) and azimuthal (u_θ) velocity profiles of the measurements (dash-dotted lines) and computational data (solid lines). The left column shows a combined plot of the axial and azimuthal velocity profiles for all downstream positions. The middle and right columns show the self-similarity scaled axial and azimuthal velocity profiles, respectively. In the case of the computations, the velocity profiles have been represented at the plane positions $z/h = 5, 15$, while the experimental profiles have been represented at $z/h = 5, 13$, according to Velte.[18] Note that these profiles all collapse nicely except on the left side of these profiles, in particular for the axial velocity, where the secondary vortex perturbation appears.

From visual inspection of the left column in Figure 9, it becomes apparent that the axial and azimuthal velocity profiles in the vortex core do not change significantly for the various angles φ. Of course, the presence of the wall and the emergence of the perturbing secondary structure create distortions in the outer regions of the core, which are particularly observable on the left side of the plots for $\varphi = 45°, 90°$ and $135°$. The computational results follow the same trend of the experiments, although some features are pronounced to a greater or lesser extent. The effects of the secondary perturbing vortex are more clearly visible on the left side of the axial velocity profiles of the experimental results for $\varphi = 0°$. Moreover, the speedup in the azimuthal velocity close to the wall for $\varphi = 90°$ is larger in the experiments compared with the computational profiles, which is consistent with the stronger induction further downstream. These anomalies can be attributed to the vortex core strength being larger in the computations (Figure 7) and the vortex core distance to

the wall being smaller in the wind tunnel experiments. More specifically, the distance from the center of the vortex to the wall in the case of the computations corresponds to 0.84 times the VG height, measured in a plane perpendicular to the wall, and five times the device height downstream of the VG, while in the experiments, it was observed that the distance from the cen- ter of the vortex to the wall at the same downstream position is only 0.72 times the VG height. The last effect can also be attributed to the vortex core size being larger in the simulations (Figure 7). A stronger primary vortex positioned closer to the wall will naturally cause stronger swirl velocities and a larger spanwise adverse pressure gradient at the wall, causing the separation (i.e., secondary vortex core) to increase in strength, hence increasing the perturbations on the primary vortex. Further, some general differences between the measured and computed velocity profiles are observed. The axial velocity

induction is not as pronounced in the computations as in the measurements. This is apparent from the smaller deficit in the wake profiles of the computations in comparison with the measured ones (Figure 9, left column). The swirl veloci- ties are also generally observed to be smaller in the computed flow. Secondly, the vortex core size (distance between the extreme swirl velocities in the right column of Figure 9) varies more than that in the measurements. The vortex core is also larger in the computations than in the measurements, as can be seen by comparing the azimuthal profiles in the left column of Figure 9.

4. DISCUSSION OF RESULTS

Although the simulations are not perfectly able to mimic the measured flow, the general trends in the flow are captured, and the simulations are able to reproduce both the helical symmetry (linear relation between the axial and azimuthal flows) and the self-similar behavior in the mean velocity profiles. The helical symmetry of the main vortex generated by a rectangular VG on a test section wall has been tested and compared with the analytical model developed in [5] with good agreement. Self-similarity behavior has also been confirmed in the computations in several positions downstream of the VG. According to Figure 9, both axial and azimuthal velocity profiles collapse for every angle γ, 0^1, 45^1, 90^1 and 135^1 so that

the full 3-D flow is covered. The computational profiles show a qualitative agreement with

the experiments in the basic physical flow response of the VG wake, although differences are more visible on the azimuthal velocities. Furthermore, as a quantitative comparison, four characteristic vortex parameters have been analyzed: convection velocity, circulation, helical pitch and vortex core radius (Figure 7). The trends of these parameters of the computational simulations are in line with the ones shown in the experiments. However, some discrepancies are visible in the values of these parame- ters. The computations overpredict the circulation and the vortex core radius, while the helical pitch is underpredicted. These discrepancies could be explained by the assumption of isotropy of the eddy viscosity models, causing problems in predicting the behavior of rotating flows. As the inflow in the simulations is assumed steady, all unsteadiness present in the actual experiment is neglected in the mean flow and must be accounted for through the turbulent eddy viscosity.

The turbulence models are designed to simulate turbulent variations in the flow and therefore may have troubles simulating the large-scale flow variations of the primary as well as secondary vortices. This can explain why the convection velocity growth rate along the streamwise direction is significantly weaker in the simulations than in the experiments. As represented in Figure 7(a), in the measurement plane positions closer to the VG, the computations overpredict the convection velocity; however, because of a higher slope of the convection velocity evolution in the experimental results, it is underpredicted in the positions far from the VG. This will naturally also affect the numerically obtained vortex core radius, circulation and helical pitch. In addition to the inlet conditions not being perfectly reproduced in the simulations, the limitations in existing turbulence model in correctly predicting such highly complex flows as the present example cannot be ignored. The flow contains strong pressure gradients in many directions with cases of separation (e.g., the secondary vortex), which are known to be notoriously difficult for the turbulence models to handle. Nevertheless, the simulations can capture the main trends of this complex, highly 3-D flow once these constants are found, and therefore, the reduced analytical model obtained from the experiments is especially valuable for these types of simulations since knowledge of the flow at one single downstream position from experiments can be used to validate the numerical simulations throughout the entire developed VG wake.

It is important to evaluate the performance of CFD methods for these types of flows, since these are, by far, the most

commonly used in practice for this type of problem. The importance of well-designed VG configurations for the total wind turbine performance and their upscaling is emphasized by the studies of Øye[13] and Miller.[14] We have in the present

study shown quantitatively that CFD can reproduce the same kind of trends that are observed in measurements. Note that, apart from the highly complex viscous interactions with secondary structures and the wall, the current model used can describe the complete flow characteristics of the VG wake. This kind of comparison has previously only been performed in a qualitative fashion or only quantitatively to some extent.

5. CONCLUSIONS

Vortices generated by a passive rectangular vane-type VG of the same height as the local

D D

D

boundary layer thickness above a test section wall have been studied. CFD simulations at Reynolds number *Re* 1700 based on the VG height *h* 0.25 m and free stream velocity *U* 1 ms^{-1} have been carried out using the RANS method and compared with wind tunnel experimental data and an analytical model.

The vortex generated by the VG shows a self-similar behavior for both the axial and azimuthal velocity profiles. It has been proven based on the computer-simulated data from five cross-plane positions *z=h* 5, 7.5, 10, 12.5 and 15 downstream of the trailing edge of a VG with an angle of attack of ˇ 20¹ to the oncoming flow, just as in the experiments. The computational results show relatively good agreement with the self-similarity shown in the experi- ments, both displayed in Figure 9 and also present in the work of Velte.[18] The trends of the characteristic helical vortex parameters in the computational results match the experimental observations reasonably well (Figure 7) considering the limitations of the turbulence models for reproducing the embedded vortices produced by vane-type VGs and the applied
inlet conditions.

From the point of view of self-similarity, computational simulations are able to reproduce the physics of the vortex generated by a rectangular VG with reasonably good reliability. Furthermore, the helical symmetry has been also tested and verified based on the computational data.

As CFD methods are the most common ones applied in optimizing VGs on wind turbine blades, the detailed information provided by the investigations of the present study can be used as a guidance for successful implementation of VGs on a wind turbine blade and to investigate parametric dependencies of the VGs on different boundary layers. Because of the vast range of parameters inherent in the problem (angle, interspacing, orientation, VG height and length, etc.), an exhaustive understanding of the flow is required to be applied properly, in which the application of this simplifying model can be helpful. Note that the current model applied can describe the complete flow characteristics of the VG wake (except for the viscous wall/secondary structures interactions) in a physical fashion and facilitates the validation of computational results. To the knowledge of the authors, this kind of comparison has previously only been carried out in a qualitative fashion or only quantitatively to some extent, i.e., only covering some aspects of the VG-induced wake.

ACKNOWLEDGEMENTS

U. F.-G. is very grateful to E. Zulueta of the University College of Engineering Vitoria-Gasteiz (UPV-EHU, Spain) for his helpful remarks. U. F.-G. is also thankful to the Government of the Basque Country by the financial support of this work through the SAIOTEK research plan (S-PE11UN112). C. M. V. and N. N. S. were supported by EUDP-2009-II-grant journal no. 64009-0279, which is also gratefully acknowledged. Computations were made by use of Thyra PC-cluster at DTU Risø Campus.

REFERENCES

1. Taylor HD. Application of vortex generator mixing principles to diffusers, *Technical Report Research Department Concluding Report No. R-15064-5,* United Aircraft Corporation, East Hartford, Connecticut, 1948.
2. Taylor HD. Design criteria for and applications of the vortex generator mixing principle, *Technical Report Research Department Report No. M-15038-1,* United Aircraft Corporation, East Hartford, Connecticut, 1948.
3. Taylor HD. Summary report on vortex generators, *Technical Report Research Department Report No. R-05280-9,*
   United Aircraft Corporation, East Hartford, Connecticut, 1950.
4. Schubauer GB, Spangenber WG. Forced mixing in boundary layers. *Journal of Fluid Mechanics* 1960; **8**: 10–32.
5. Velte CM, Hansen MOL, Okulov VL. Helical structure of longitudinal vortices embedded in turbulent wall-bounded flow. *Journal of Fluid Mechanics* 2009; **619**: 167–177.
6. van RR, Timmer WA. Roughness sensitivity considerations for thick rotor blade airfoils. *Journal of Solar Energy Engineering—Transactions of the ASME* 2003; **125**: 468–478.
7. Lin JC. Review of research on low-profile vortex generators to control boundary layer separation. *Progress in Aerospace Sciences* 2002; **38**: 389–420.
8. Pearcey HH. Shock induced separation and its prevention by design and boundary layer control. In *Boundary Layer and Flow Control.* G. V. Lachmann (ed.). Vol. 2. Pergamon Press, 1961, 1166–1344.
9. Kerho M, Huctcherson S, Blackwelder RF, Liebeck RH. Vortex generators used to control laminar separation bubbles.
   Journal of Aircraft 1993; **30**: 315–319.
10. Wendt BJ. Parametric study of vortices shed from airfoil vortex generators. *AIAA Journal*

2004; **42**: 2185–2195.

11. Ashill PR, Fulker JL, Hackett KC. Research at DERA on sub boundary layer vortex generators (SBVGs). *39th Aerospace Sciences Meeting and Exhibit, AIAA*, Reno, Nevada, January 2001; 8–11.
12. Ashill PR, Fulker JL, Hackett KC. Studies of flow induced by sub boundary layer vortex generator s (SBVGs). *40th Aerospace Sciences Meeting and Exhibit, AIAA*, Reno, Nevada, January 2002; 14–17.
13. Øye S. The effect of vortex generators on the performance of the ELKRAFT 1000 kW turbine. *9th IEA Symposium on Aerodynamics of Wind Turbines*. ISSN, Stockholm, Sweden, 1995; 0590–8809.
14. Miller GE. Comparative performance tests on the Mod-2, 2.5-MW wind turbine with and without vortex generators.
    DOE/NASA Workshop on Horizontal Axis Wind Turbine Technology. Cleveland, OH, United States, 1984; 8–10.
15. Smith FT. Theoretical prediction and design for vortex generators in turbulent boundary layers. *Journal of Fluid Mechanics* 1994; **270**: 91–131.
16. Bender EE, Anderson BH, Yagle PJ. Vortex generator modeling for Navier–Stokes codes. *Proceedings of the 3rd ASME/JSME Joint Fluids Engineering Conference*, San Francisco, California, USA. EDSM 99-6919, 1999.
17. Alekseenko SV, Kuibin PA, Okulov VL. Theory of concentrated vortices. An Introduction, (1st edn). Springer-Verlag: Berlin Heidelberg, 2007.
18. Velte CM. A vortex generator flow model based on self-similarity. *AIAA Journal* 2013; **51**(2): 526–529.
19. White FM. Viscous Fluid Flow (2nd edn). McGraw-Hill: Singapore, 1991,470–481.
20. Michelsen JA. Basis3D—a platform for development of multiblock PDE solvers, *Technical Report AFM 94-06*, Technical University of Denmark, Department of Mechanical Engineering, Denmark, 1994.
21. Sørensen NN. General purpose flow solver applied to flow over hills, *Technical Report Risoe-R-827(EN),* Risoe National Laboratory, Denmark, 1995.
22. Khosla K, Rubin SG. A diagonally dominant second-order accurate implicit scheme. *Computer Fluids*, 1974; 207–209.
23. Menter FR. *Zonal two equation k – ! turbulence model for aerodynamic flows.* AIAA Journal, (93-2906), 1993.

24. Allan BG, Chung-Sheng YC, Lin JC. Numerical simulations of vortex generators and jets on a flat plate. *1st Flow Control Conference, AIAA*, St. Louis, Missouri, June 2002; 24–27.
25. Fernández U, Réthoté P-E, Sørensen NN, Velte CM, Zahle F, Egusquiza E. Comparison of four different models of vortex generators. *Proceedings of EWEA—European Wind Energy Conference*. Copenhagen, 2012; 16–19.
26. Velte CM. Characterization of vortex generator induced flow, *PhD Thesis*, Denmark, 2009.
27. Vinokur M. On one-dimensional stretching functions for finite-difference calculations. *Journal of Computational Physics* 1983; **50**: 215–234.
28. Godard G, Stanislas M. Control of a decelerating boundary layer. Part 1: optimization of passive vortex generators.
Aerospace Science and Technology 2006; **10**: 181–191.